PERGAMON

International Journal of Solids and Structures 38 (2001) 2049–2068

INTERNATIONAL JOURNAL OF SOLIDS and STRUCTURES

www.elsevier.com/locate/ijsolstr

Spatio-temporal dimensionality in the overall complex dynamics of an experimental cable/mass system

Giuseppe Rega [a,*], Rocco Alaggio [b]

[a] *Dipartimento di Ingegneria Strutturale e Geotecnica, Università di Roma La Sapienza, via A. Gramsci 53, 00197 Roma, Italy*
[b] *Dipartimento di Ingegneria delle Strutture, Acque e Terreno, Università dell'Aquila, Monteluco Roio, 67040 L'Aquila, Italy*

Received 9 August 1999; in revised form 13 December 1999

Abstract

An experimental model of an elastic cable/mass hanging at in-phase or out-of-phase vertically moving supports is considered. System parameters are adjusted to produce two different conditions of multiple internal resonance. Nonregular dynamics are analyzed in various frequency ranges including meaningful external resonance conditions. Attention is devoted to characterization of system dimensionality in terms of both time and spatial complexity. The aims of this paper are (i) to give a general overview of the richness and robustness of different (quasiperiodic and homoclinic) bifurcation scenarios to chaos in various regions of the control parameter space, (ii) to characterize steady nonregular response through delay-embedding technique for attractor reconstruction and proper orthogonal decomposition of spatio-temporal flow and (iii) to identify spatial configuration variables (experimental eigenfunctions) contributing mostly to nonregular dynamics, thus obtaining hints about possible reduced models for reproducing complex regimes. System dimensionality will be evaluated both by relating the dimension of attractors to the dimension of the linear phase space, and from the dominating proper orthogonal modes.

Keywords: Experimental nonlinear dynamics; Bifurcation; Chaos; Proper orthogonal modes; Reduced models; Cables

1. Introduction

In applied solid mechanics, when dealing with multidegrees-of-freedom or continuous systems undergoing finite amplitude vibrations, there is a strong possibility of response regimes involving several spatial modes in either regular or complex nonlinear behavior. Reliable and complete descriptions of many possible regimes in control parameter space have to be obtained through systematic experimental investigations on physical models of the considered system. Rich and varied response charts exhibiting several regions of different classes of motion are usually obtained, depending also on the realization of meaningful external and/or internal, and possibly multiple, resonance conditions.

* Corresponding author. Fax: +39-06-322-1449.
E-mail address: rega@dsg.uniromal.it (G. Rega).

0020-7683/01/$ - see front matter
PII: S0020-7683(00)00152-9

Quasiperiodic and chaotic motions are seen to occur mostly in between regions of clearly dominating low-dimensional regular responses. One major effort in experimental analysis consists of properly characterizing the bifurcation mechanisms leading to complex attractors, and the attractors themselves, from the point of view of the *dimension* of the dynamics. Indeed, investigating the possible finite dimensionality in the complex dynamics of potentially infinite-dimensional systems, and detecting minimum numbers and features of configuration variables actually needed to describe such complex motions, are important questions in nonlinear dynamics (Cusumano et al., 1994; Steindl et al., 1999; Georgiou and Schwartz, 1999).

Dimensionality has to be characterized in terms of both *time complexity* and *spatial complexity*. The former characterization is accomplished by calculating invariant measures of the dynamics (including strangeness and chaoticity) through the delay embedding procedure (Packard et al., 1980; Takens, 1981; Mané, 1981; Sauer et al., 1991): this is done in a reconstructed phase space being in a one-to-one (topological and dynamical) correspondence, under certain reconstruction conditions, with the real, high-dimensional, but inaccessible phase space. The embedding procedure is of special interest just for allowing reliable estimations of system dimensionality: indeed, it gives indications on the actual number of degrees-of-freedom (dof) taking meaningful part in the system nonlinear response (Eckmann and Ruelle, 1985).

Spatial complexity, on the other hand, is characterized by identifying the configurations that are most visited, on average, during a spatio-temporal evolution. This is best done through the proper orthogonal decomposition (POD) or Karhunen–Loeve procedure (Holmes et al., 1996) based on spatial coherence analysis. The POD allows us to characterize the response not only in terms of the number of dof involved (as per the embedding procedure) but also with respect to their mechanical meaning (spatial shape). Moreover, it furnishes the optimal basis to decompose the spatial flow, and thus a suitable basis for projecting a continuous theoretical model through some analytical reduction technique.

The present paper illustrates and discusses the above mentioned topics with reference to elastic mono-dimensional systems in solid and structural mechanics. The application of POD is based on the availability of spatially contemporaneous measures, and so a distinction has to made between systems with bending stiffness (beams and arches) and flexible systems with negligible bending stiffness, such as suspended cables. Contact measurement sensors (e.g. accelerometers) can be used in the former case, while no-contact and currently expensive optical/laser sensors resulting in very low number of synchronous measures, are required in the latter case. Yet, flexible systems are of special interest, owing to the combined effect of flexibility, which naturally entails involved 3D responses, and possibly high modal density enhancing involvement of several modes in highly coupled nonlinear responses.

In this paper, an experimental model of elastic cable with concentrated masses hanging from two supports moving vertically and sinusoidally in-phase or out-of-phase is considered (Fig. 1) (Rega et al., 1997). For relatively low frequency of the support motion, a reliable model of bare suspended cable is realized. The in-plane (vertical) and out-of-plane (horizontal) cable/mass linear modes are labeled Vn and Hn, respectively (n = odd, symmetric; n = even, antisymmetric) (Fig. 1(a)). The mechanical and geometrical properties of the system realize a condition of 2:2:1 multiple internal resonance involving the frequencies $\omega(\cdot)$ of the first antisymmetric in-plane (V2) and out-of-plane (H2) modes, and of the first symmetric out-of-plane (H1) mode.

Previous papers, mainly devoted to characterization of regular response (Rega et al., 1997; Benedettini and Rega, 1997) furnished local and global descriptions of the system dynamics. Overall response charts in excitation parameter space were obtained, showing the existence of quite large regions of quasiperiodic and chaotic motion for forcing frequencies close to meaningful external resonance conditions. In-depth analyses of a meaningful scenario to chaos occurring in a specific region of parameter space have then been made in (Alaggio and Rega, 2000a). General aims of the present work are instead (i) to give a general overview of the richness and robustness of bifurcation scenarios in various regions, (ii) to characterize different mechanisms of transition to nonregular dynamics and (iii) to identify possible reduced models for complex

(a)

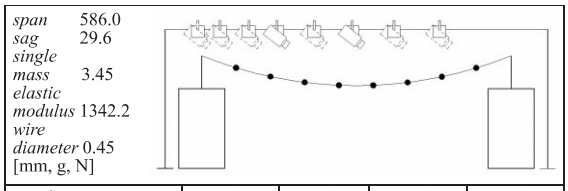

mode	H1	V2	H2	V1
shape h-plane				
shape v-plane				
frequency ω [Hz]	3.49	6.68	6.77	8.82
damping	0.0021	0.0003	0.0008	0.027

(b)

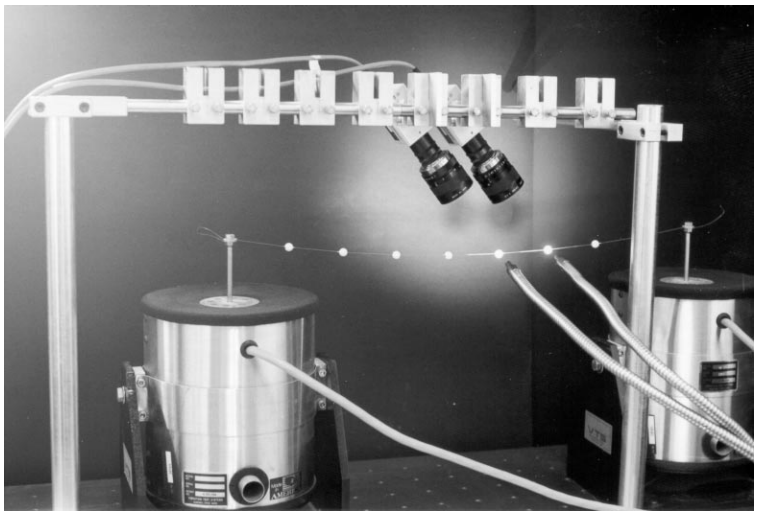

Fig. 1. (a) Sketch of the mechanical model with its parameters and dynamical characteristics. (b) The hanged nylon wire carrying eight concentrated masses, the shakers and the two movable optical cameras.

regimes from experimental observations, thus obtaining hints for the construction of corresponding minimal theoretical models able to reproduce those behaviors.

In the framework of spatio-temporal characterization of most robust classes of motion, particular attention will be devoted (i) to characterize the relevant steady attractors in terms of dimensionality, strangeness, and possible chaoticity and (ii) to identify the experimental eigenfunctions (proper orthogonal modes, POMs) mostly contributing to nonregular dynamics, and their mechanical meaning.

Besides Poincaré map inspection and power spectra analysis, information about dimension of quasi-periodic and chaotic attractors will be obtained from correlation dimension evaluations (Grassberger and Procaccia, 1983) carried out on time-delayed reconstructed phase spaces using one or two simultaneous experimental time series (Abarbanel et al., 1993; Broomhead and King, 1986). Information about chaoticity will be obtained through maximum Lyapunov exponent evaluations (Holzfuss and Lauterborn, 1989).

The investigated scenarios evolve in a potentially infinite-dimensional phase space. Attractors of same dimension can of course lie on different manifolds: characterizing the invariant manifolds where the motion

actually develops, with lower dynamical dimension, is thus of a major interest for reliable motion classification. In this respect, the bare attractor dimension criterion does not allow us to distinguish, e.g., between a phase-locked periodic response involving several cable modes and a single-mode response. Therefore, informations relevant to topology and dimension of invariant manifolds are also needed as a further important classification criterion of the dynamics.

The number and kind of participating configuration variables will be identified through orthogonal decomposition of the discrete covariance matrix obtained from two-by-two spatial correlations of time laws of two masses simultaneously acquired in stationary regime (Alaggio and Rega, 2000a).

System dimensionality will be tackled by following two approaches. On the one hand, it will be evaluated on reconstructed attractors by relating their dimension to the dimension of the linear phase space. On the other hand, it will ensue from the analysis of the spatial structure of nonregular flows and of the relevant dominating experimental eigenfunctions.

System transition from regular to nonregular dynamics will be investigated in primary and 1/2-subharmonic external resonances for either in-phase or out-of-phase support motion. Nonregular behavior of the model will be seen to be very rich and varied. Nevertheless, the observed bifurcation paths will be traced back to *canonical scenarios* of dynamical system theory, which are here sometimes simultaneous and competing with each other. In particular, the quasiperiodic (3-tori breakdown) scenario will be discussed in Section 2, first summarizing the results discussed in detail in (Alaggio and Rega, 2000a) for the sake of completeness (Section 2.1), and then extending the description to a different external resonance condition (Section 2.2). A scenario involving the global bifurcation of an homoclinic invariant set of the flow will be analyzed in Section 3. In both cases, peculiar and/or persistent bifurcation features exhibited in each considered case of resonance-zone/support-motion will be discussed. Robustness of the two scenarios as observed for the reference experimental cable (labeled slacker cable in the following) will also be checked towards variations of the system mechanical parameters, by considering a cable involving in a 2:2:1:2 resonance the first in-plane symmetric mode (V1), too: it corresponds to a cable at first crossover of the in-plane symmetric and antisymmetric natural frequencies (Irvine and Caughey, 1974; Benedettini et al., 1995). A general discussion of the highlighted bifurcation paths will conclude the paper (Section 4), with a summary and comparison of indications obtained in terms of dimensionality and mechanical content of the system dynamics.

2. Tori breakdown scenario

A bifurcation path in which chaos onsets following successive Hopf bifurcations increasing the attractor dimension is typical of high-dimensional dissipative dynamical systems. Quasiperiodic transition to chaos received interest in the last decades since the early works by Ruelle and Takens (1971) and by Newhouse et al. (1978). The latter showed that chaotic attractors could arise from 3-T-quasiperiodic flows on 3-torus as a consequence of arbitrarily small perturbations. Subsequent investigations by Grebogi et al. (1985) cleared up the NRT scenario to be unlikely in typical physical systems. Numerical investigations about transition to chaos of flows on 3-tori frequently showed the case in which destruction of torus precedes incoming of chaos (Battelino et al., 1989; Giberti and Zanassi, 1993). More recently, Baesens et al. (1991) furnished a detailed analysis of bifurcation behavior of flows on 3-tori, and Anishchenko et al. (1994) investigated 3-torus breakdown numerically, extending previous results relevant to 2-torus. The *quasiperiodic* scenarios observed in the experimental cable/mass originate from 3-tori breakdown.

A series of homogenous classes of motion is singled out in the sequence of bifurcations to chaos. Their classification is made based on topological dimension of manifolds where motion develops (growing, in regular regime, from one to three-torus) and on correlation dimension of attractors (from one to three in regular regime, coinciding with their local topological dimension; noninteger in chaotic regime). Accord-

ingly, regular motions are labeled Pm[-Mk]: periodic, nT-QPm[-Mk]: quasiperiodic. Labels give information on the attractor (m: periodicity, n: number of incommensurate frequencies equal to correlation dimension) and manifold dimensions (equal to n for quasiperiodic – one for periodic – if not differently specified by k in the case of partially or totally resonant, i.e., nonergodic, tori).

The QP scenario is responsible for transition to chaos in the slacker cable around nominal primary and 1/2-subharmonic resonance of the reference first in-plane antisymmetric mode V2 under in-phase and out-of-phase support motion, respectively.

2.1. In-phase support motion, primary resonance

This case was analyzed in-depth in (Alaggio and Rega, 2000a) for the slacker cable. Herein, the main features of the overall scenario are summarized, and meaningful aspects of spatio-temporal dimensional characterization of most important classes of motion are presented.

The behavior shown by the system is very rich and varied showing regular and nonregular solutions, and involved bifurcation mechanisms. All phenomena originate from participation to response of up to three incommensurate frequencies. Upon developing of system dynamics on a 3-torus (as a consequence of two Hopf bifurcations), further varying the control parameter entails 3T-quasiperiodic motion, torus breakdown with transition to chaos, and phase-locked quasiperiodic and high-periodicity solutions.

The bifurcation analysis is performed by varying the forcing frequency and keeping the forcing amplitude constant at a value 1.0 V (0.17 mm of support motion, cfr. relevant behavior chart, Fig. 2, in Benedettini and Rega, 1997). The schematic bifurcation diagram in Fig. 2 shows the main phenomena occurring in the range 1.155–1.250 of values of the adimensional frequency $\Omega^* = \Omega/\omega(\mathrm{V2})$, where the complex dynamics develop, Ω being the excitation frequency and ω(V2), the natural frequency of the first in-plane antisymmetric mode V2.

In the overall transition region, the model shows a close- and intertwined-sequence of regular and nonregular response classes: (i) two-frequency quasiperiodic motions on two-dimensional manifolds (2T-QP1), (ii) two-frequency phase-locked quasiperiodic motions on three-dimensional manifolds (2T-QP2-M3), (iii) stable three-frequency quasiperiodic motions (3T-QPm), (iv) chaotic motions (CH1, CH2) and (v) phase-locked periodic motions which are invariant sets of dimension 1 on three-dimensional manifolds (Pm-M3).

Accordingly, various types of bifurcation occur: (i) Hopf bifurcation from 2T-quasiperiodic (on a 2-torus-2T-QP1, as well as phase-locked on a 3-torus-2T-QP2-M3) to stable 3T-quasiperiodic (with two

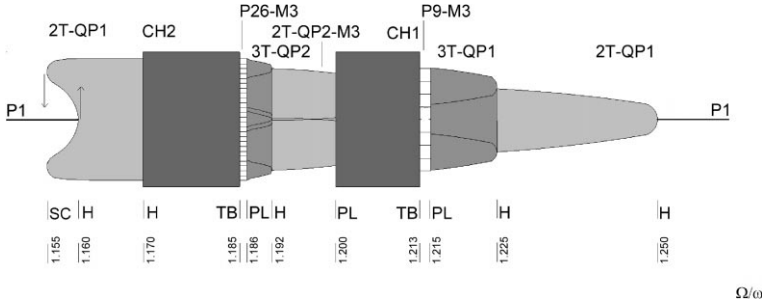

Fig. 2. Schematic bifurcation diagram (in-phase support motion, primary resonance). H: Hopf, PL: phase-locking, TB: torus breakdown, SC: saddle cycle. The highlighted motion classes refer to periodic (Pm[-M3]), quasiperiodic (nT-QPm[-M3]) and chaotic (CH1, CH2) attractors.

Table 1
An overview of the motion class characterization[a]

Attractor	Dimension						Modes
	D_C	D_S	D_E	D-T	No. POMs	D_P	
In-phase support motion – primary resonance							
P1	1	2	$1 \div 3$	1	1 (96.4%)	3	V1
2T-QP1	2	3	$2 \div 5$	2	2 (98.7%)	5	V1 H1
2T-QP1 (fuzzy)	2.12	7	$3 \div 7$		2 (98.1%)	5	V1 H1
					3 (98.9%)	7	V1 H1 H2
2T-QP2-M3	2	4	$2 \div 5$	3^R	3 (98.8%)	7	V1 H1 H2
3T-QP1 (3T-QP2)	3	6	$4 \div 7$	3	3 (98.4%)	7	V1 H1 H2
P9-M3, P26-M3	1	3	$1 \div 3$	3^R		7	V1 H1 H2
CH2	3.45	9	$4 \div 9$		3 (91.5%)	7	V1 H1 H2
					4 (94.2%)	9	V1 H1 H2 H3
CH1	2.27	7	$3 \div 7$		2 (94.7%)	5	H1 H2
					3 (95.5%)	7	V1 H1 H2

[a] D_C is the attractor estimated correlation dimension, D_S is the embedding dimension corresponding to dimension invariant saturation, D_E is the expected embedding dimension variation range according to the relationship $[D_C] \leqslant D_E \leqslant (2[D_C] + 1)$, where [ ] means the nearest greater integer (the upper bound limit is given by the Mané theorem), D-T column shows the dimension of possibly resonant (R) invariant tori if it exists, No. POMs column shows the number of experimental eigenfunctions identified and the relevant signal power percentage, D_P is the dimension of phase-space required to display the main system dynamics, last column lists the natural cable/mass modes to whom the experimental eigenfunctions can be referred.

topologically different 3T-QPm motions), (ii) transition from stable 3T-QPm to chaotic attractors through 3-tori breakdown and (iii) phase-locking of chaotic motion on 2T-QP2-M3 attractor, and of 3T-QPm motions on high periodicity solutions.

The underlying outside period 1 response having correlation dimension $D_C = 1$ (Table 1) is dominated by the first symmetric in-plane mode (V1) of the cable/mass, which is excited in primary resonance ($\omega^*(V1) = \omega(V1)/\omega(V2) = 1.32$). This is clearly shown (Alaggio and Rega, 2000a) by the high signal power content ($\varphi = 96.4\%$) pertaining to the relevant first POM, which has an in-plane component directly referable to V1 while negligible out-of-plane component.

Involvement of further modes in the system dynamics within the frequency range is associated with nearness of first symmetric out-of-plane mode H1($\omega^*(H1) = 0.52$) to its order 1/2-subharmonic resonance and of first antisymmetric out-of-plane mode H2 ($\omega^*(H2) = 1.01$) to its primary resonance (Rega et al., 1997). Going inside the 1.155–1.25 range, a Hopf bifurcation – subcritical for increasing frequency and supercritical for decreasing frequency, respectively – drives the asymptotic response onto a 2-torus, as revealed by the Poincaré section inspection (Fig. 3(a)) and by the correlation dimension $D_C = 2$. The first two POMs, normalized to unity, containing very high percentage (φ) of signal power, are shown in Fig. 3(b). Both in-plane and out-of-plane components are represented. The two main configuration variables involved in the response are identified as the first symmetric out-of-plane (H1) and in-plane (V1) modes of the cable.

The 2T-quasiperiodic motion identified by the label 2T-QP1 is stable only at the borders of the overall frequency range. Going further inside this range, the system exhibits rich behavior due to the involvement in the response of a third harmonic of incommensurate frequency with respect to the two ones already involved in the 2T-quasiperiodic. In fact, with decreasing frequency, two successive secondary Hopf bifurcations drive the system to 3T-quasiperiodic attractors (3T-QP1 and 3T-QP1, respectively, with correlation dimension $D_C = 3$) followed by narrow stripes of intermittent phase locking on P9-M3 and P26-M3 periodic solutions and, finally, by wide ranges (CH1, CH2) of chaotic behavior.

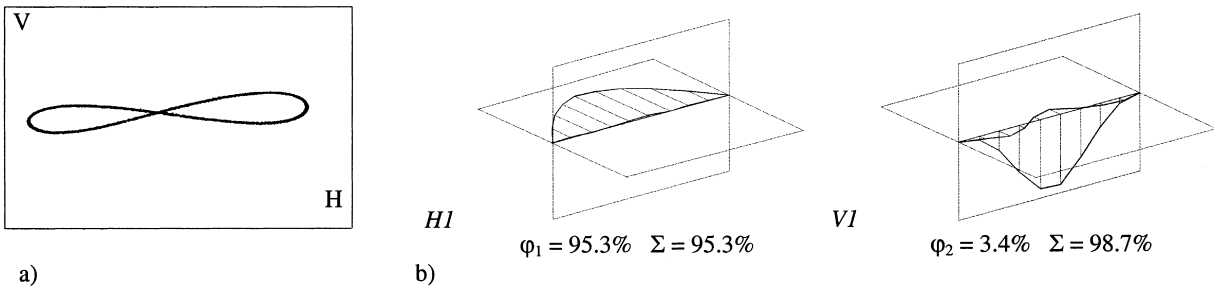

Fig. 3. (a) Poincaré section of the configuration space. (b) First two proper orthogonal modes.

The coherence analysis identifies the third configuration variable responsible for further incommensurability as the first antisymmetric out-of-plane mode (H2). This mode plays an important role in all of the different motion classes occurring on the two successive 3-tori.

Although involving same cable modes and having same attractor dimensions, the two classes (3T-QP1, 3T-QP2) of 3T-quasiperiodic responses are topologically different because they bifurcate from different 2T-quasiperiodic motions: the first (2T-QP1) laying on an ergodic 2-torus, the second (2T-QP2) laying on a partially resonant 3-torus. Their Poincaré maps are shown in Fig. 4(a) and (b).

The coherence analysis (POMs in Fig. 4(c)) highlights the role played in 3T-quasiperiodic motions by the two out-of-plane modes (symmetric and antisymmetric): in particular, the power associated with the first antisymmetric out-of-plane mode (H2) now exceeds the contribution of the first symmetric in-plane mode (V1).

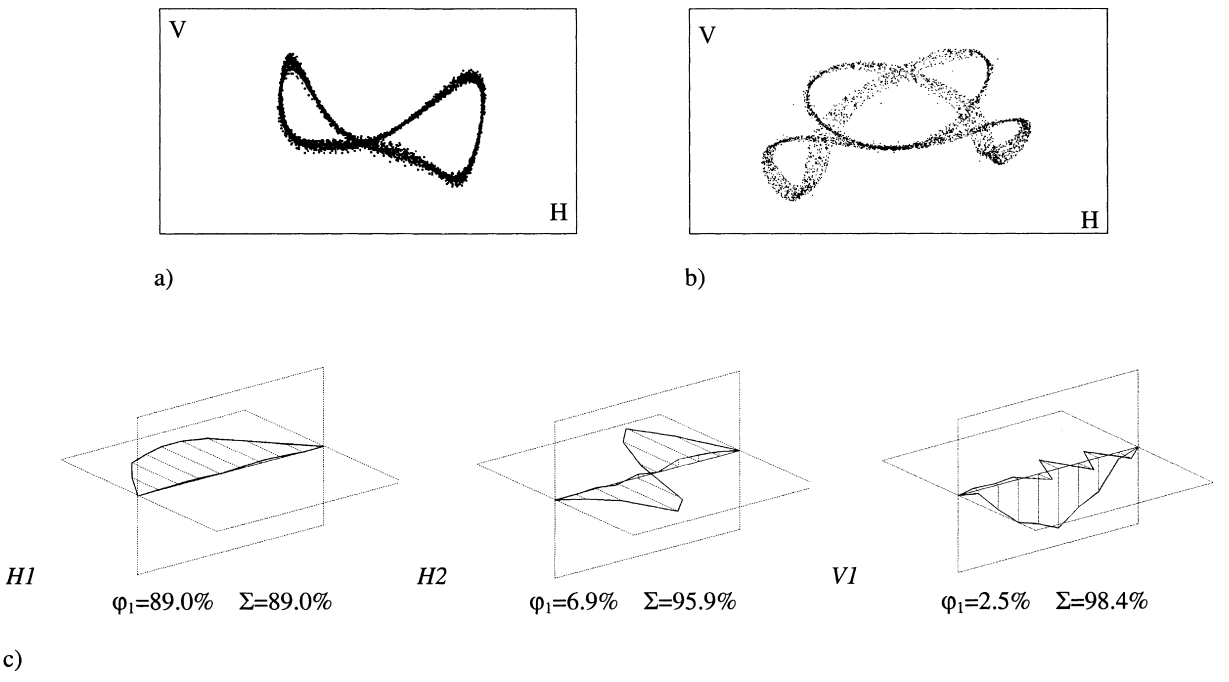

Fig. 4. Poincaré sections relevant to (a) 3T-QP1 and (b) 3T-QP2 motion classes. (c) First three POMs relevant to 3T-QP1.

The two chaotic regions (CH1, CH2) in the schematic bifurcation diagram of Fig. 2 are entered from zones where the dynamics lie on a 3-torus. An experimental realization in region CH2 exhibits the continuous power spectrum and Poincaré map projection displayed in Fig. 5(a) and (b), respectively. A dominant double period is observed, and the chaotic steady nature of the response is confirmed by both the fractal value $D_C = 3.45$ and the positive value 0.108 calculated for the maximum Lyapunov exponent. A realization in region CH1 (Fig. 5(c) and (d)) shows the dominant basic period and lower correlation dimension value ($D_C = 2.27$), which increases however when moving towards the left boundary of the region.

The major spatial shapes identified through the coherence analysis are shown in Fig. 6(a) and (b) for the CH2 and CH1 case, respectively. The basic POMs corresponding to the first in-plane and out-of-plane symmetric modes of the cable are again clearly recognizable, however, with exchanged relative power content in the two cases. A third POM, very similar to the first antisymmetric out-of-plane mode takes, also, meaningful part in the two responses with comparable power.

In the middle part of the experimental diagram, the motion belongs to a 2T-quasiperiodic attractor ($D_C = 2$) of double period (2T-QP2-M3), the M3 label denoting a phase locking phenomenon on the 3-torus. This phase-locked motion is characterized by a spatial flow to be decomposed in a linear phase space using at least three configuration variables (M3) with phase-locked time coefficients. The relevant first three POMs ($\varphi_1 = 73.16\%,\ \varphi_2 = 20.75\%,\ \varphi_3 = 4.45\%$) are referable to H1, V1 and H2, respectively.

Restricting ourselves to the regular regime, we can notice that in the frequency range 1.225–1.170, even if the dimension of succeeding attractors varies from 1 to 3, the topological dimension of the associated manifold is always three and the number of active configuration variables (having direct counterpart in the space of cable natural modes) is always three, too.

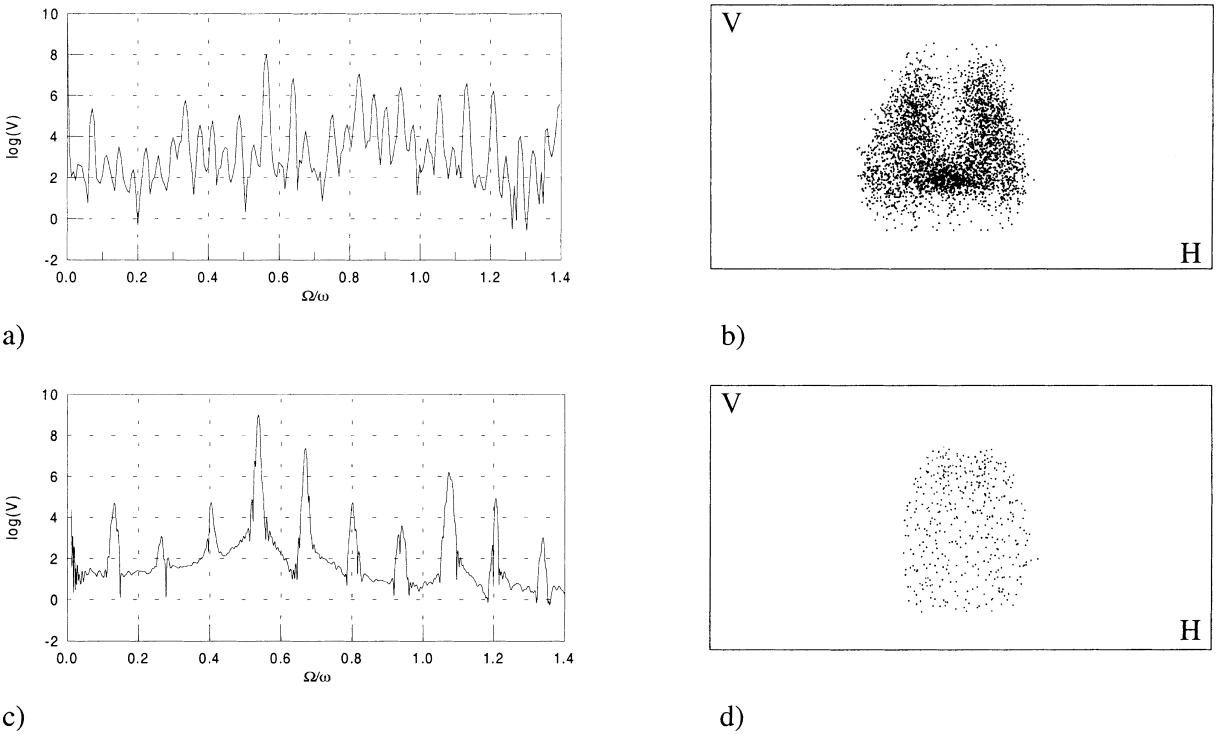

Fig. 5. (a) Power spectrum of orizontal component and (b) Poincaré section projection for CH2 motion. (c, d) Same for CH1 motion.

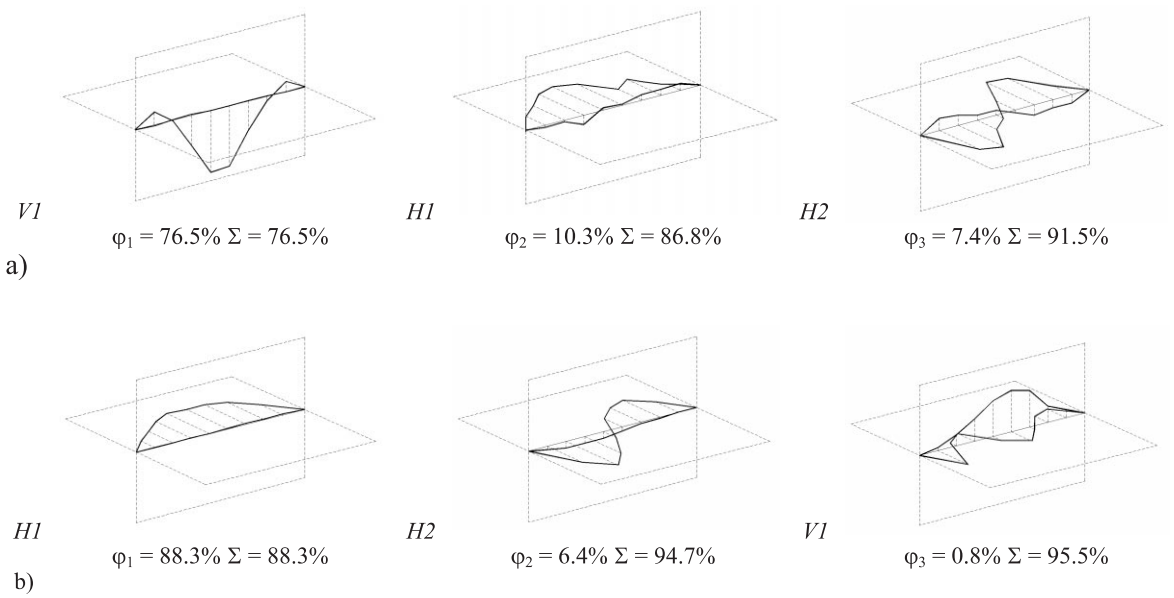

Fig. 6. (a) First three POMs relevant to CH2 and (b) CH1 motion classes.

Looking jointly at the results relevant to regular motions and chaos, the main role played by the antisymmetric out-of-plane mode H2 in transition to chaos is clearly deduced. Of course, some higher modes are involved in the fully developed chaotic attractor, too, though at lower power levels. It is worth noting that, in a theoretical model accounting only for V1, H1 and H2 (as in Benedettini et al., 1995, where V2 also, here unnecessary, is considered), 91.5% of the flow total power would be captured.

Table 1 summarizes the quantitative and qualitative information concerned with dimensionality and mechanical content of the classes of motion recognized in the quasiperiodic (torus breakdown) scenario to chaos. Dimensionality is evaluated either directly on the reconstructed attractors or indirectly from the results of spatial coherence analysis. In particular, comparison can be made between the upper bound (Mané, 1981) given by the relation $[D_C] \leqslant D_E \leqslant (2[D_C] + 1)$ ([ ] means the nearest integer greater than) involving the correlation dimension (D_C) and the embedding dimension (D_E), and the phase space dimension (D_P) in R^N, evaluated, using POD results, as two times the number of identified POMs plus 1 (the time).

In spite of the varied dynamics, the results obtained from systematic characterization of each class of motion allow us to set the bifurcation behavior of the experimental system in the framework of quasiperiodic scenario to chaos and, more specifically, of the scenario of bifurcation of flow on 3-tori and its breakdown (Baesens et al., 1991; Anishchenko et al., 1994; Alaggio and Rega, 2000a).

This scenario does not occur in the corresponding frequency range for the cable at nearly crossover condition. Indeed, the closer internal resonance conditions of the latter prevent quasiperiodic couplings from occurring, while often replacing them in parameter space with wider resonant periodic couplings, and thus also the associated quasiperiodic transition to chaos from taking place.

2.2. Out-of-phase support motion, 1/2-subharmonic resonance: quasiperiodic scenario

The response chart relevant to the slacker cable under out-of-phase support motion at 1/2-subharmonic resonance exhibits a wide range of nonregular regime (see Fig. 4 in Benedettini and Rega, 1997). The

analysis demonstrates the system nonregular dynamics in this zone to be produced by two coexisting and competing scenarios. In fact, two bifurcation paths to chaos differentiate themselves starting from the same periodic motion class, an antisymmetric ballooning solution (P1-M2) involving – in primary resonance – the second in-plane (V4) and out-of-plane (H4) antisymmetric modes of the cable.

The two scenarios produce attractors differing for dimension and spatial flow composition. The first one involves a series of Hopf bifurcations (each one drawing a new configuration variable into the response) and, again, it can be traced back to a torus-breakdown onset of chaos. The second scenario ends in a global bifurcation involving an homoclinic invariant without involving further modes. The two coexixting scenarios are characterized by different robustness with respect to variations of cable geometric-mechanical parameters, as it will be discussed later on. In this section, we show the main global results relevant to the first, quasiperiodic, bifurcation path reported schematically in Fig. 7(a) obtained for a forcing amplitude equal to 900 mV (0.2 mm of support motion) and the range 1.860–1.994 of values of the adimensional frequency $\Omega^* = \Omega/\omega(\mathrm{V2})$. The coexisting homoclinic scenario (Fig. 7(b)) will be discussed in Section 3.

Generally speaking, a more uniformly nonregular behavior is herein observed with respect to the one exhibited in the neighborhood of primary resonance condition with in-phase support motion. This is likely due to the sudden involvement of an higher number of configuration variables in the complex response originated from torus-breakdown, which prevents the system from exhibiting the complicated frame of regular and nonregular solutions observed in that case.

For growing forcing frequency, two Hopf bifurcations occur, the first one giving rise to the 2T-quasiperiodic response labeled 2T-QP(1) (and 2T-QP(2), after a jump to an higher amplitude response), the second one bringing the dynamics from two- to three-dimensional torus (3T-QP). This manifold is then soon broken, resulting in nonregular regime.

Two frequency ranges can be distinguished in the nonregular region, in each of which there is a rather smooth increase of noninteger dimension of the chaotic attractor. They are separated by a threshold value beyond which the dimension suddenly increases, thus highlighting the occurrence of a meaningful global bifurcation in the system complex dynamics: and in fact new configuration variables (identified through the POD procedure) have entered the spatial response.

Herein, we discuss some synthetic aspects concerned with spatio-temporal characterization of the dynamics in terms of dimensionality and contributing variables.

The basic periodic response is produced by the coupling of second antisymmetric in-plane (V4) and out-of-plane (H4) modes (excited in primary resonance, $(\omega^*(\mathrm{V4}) = 1.94,\ \omega^*(\mathrm{H4}) = 1.95)$, Rega et al., 1997).

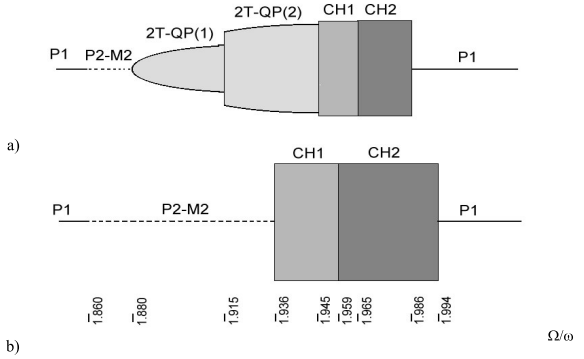

Fig. 7. Two coexisting schematic bifurcation diagrams (out-of-phase support motion, 1/2-subharmonic resonance): (a) quasiperiodic scenario and (b) homoclinic scenario.

Successive involvement of further modes in system dynamics at higher excitation frequencies is justified by nearly simultaneous proximity of excitation frequency, in a narrow range, to the 1/4-subharmonic resonance of the first torsion-symmetric mode $H1^T$ ($\omega^*(H1^T) = 0.48$) and of the first symmetric out-of-plane mode H1 ($\omega^*(H1) = 0.52$), as well as to the 1/2-subharmonic resonance of the first antisymmetric out-of-plane (H2) and in-plane (V2) modes.

Going inside the aforesaid range, a supercritical Hopf bifurcation (1.880) drives the asymptotic response onto a 2-torus. The ensuing 2T-QP motion involves (as highlighted by the POD) the two antisymmetric (V4, H4) and the first torsion-symmetric ($H1^T$) modes.

Further increasing the frequency (1.915), the system exhibits, at first, an higher response amplitude seemingly corresponding to a jump onto an upper frequency-response branch of the same 2T-quasiperiodic solution, and then (1.945) a Hopf bifurcation to a three-dimensional torus. Transition to the higher dimensional manifold looks like being due to the involvement of the first symmetric out-of-plane mode which drives into the response, further harmonic components responsible for a second incommensurability relationship.

In this case, the POD does not help in identifying the new contribution, since the modal shapes of H1 and $H1^T$ are substantially the same except for the occurrence of a torsional component in the latter (Rega et al., 1997). Their simile prevents the decomposition to distinguish between them in a configuration space where only vertical and horizontal components of motion are measured and represented: indeed, the mass rotation around the cable axis is not detected by the transducers.

Inside the nonregular region, the chaotic attractors (CH1 and CH2) occurring in two distinguished ranges have correlation dimension values varying between 3.2 and 3.6 and between 4.1 and 4.8, respectively. The following exemplifying case (spectrum and Poincaré map in Fig. 8(a) and (b)) is relevant to an attractor obtained in region CH2.

The involvement of important 1/2-subharmonic components differentiates the CH2 from the CH1 zone. In particular, the POD identifies the presence of a further configuration variable in the response, where the first out-of-plane mode H2 (close to its 1/2-subharmonic resonance) can be recognized. The first four POMs, already sufficient to decompose 89.4% of the power, are reported in Fig. 8(c) for the higher

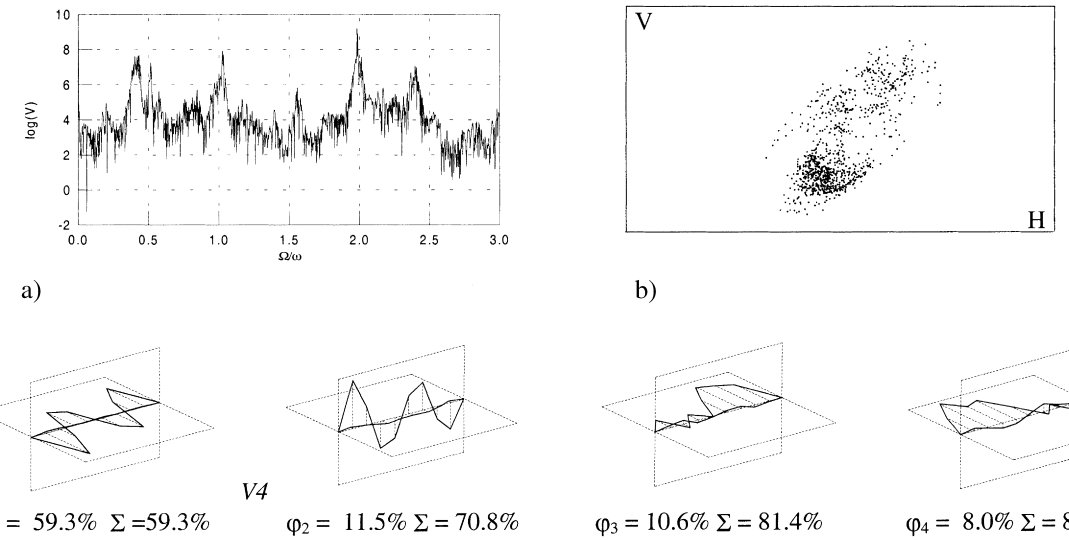

Fig. 8. (a) Power spectrum of horizontal component and (b) Poincaré section projection for CH2 motion in the quasiperiodic scenario. (c) Corresponding first four POMs.

Table 2
An overview of the motion class characterization[a]

Attractor	Dimension						Modes
	D_C	D_S	D_E	D-T	No. POMs	D_P	
Out-of-phase support motion – 1/2 subharmonic resonance quasiperiodic scenario							
P1-M2	1	2	$1 \div 3$	2^R	2	5	V4 H4
2T-QP1(a)	2	$3 \div 4$	$2 \div 5$	3^R	3 (97.8%)	7	V4 H4 $H1^T$
2T-QP1(b)	2	$3 \div 4$	$2 \div 5$	3^R	3 (97.0%)	7	V4 H4 $H1^T$
CH1	$3.2 \div 3.6$	6	$4 \div 9$		3 (96.1%)	7	V4 H4 $H1^T$
CH2	$4.1 \div 4.8$	$11 \div 12$	$5 \div 11$		4 (89.4%)	9	V4 H4$H1^T$ H2
					5 (92.5%)	11	V4 H4 $H1^T$ H2 H3
					6 (95.0%)	13	V4 H4 $H1^T$ H2 H3 V2

[a] Refer footnote of Table 1.

dimension CH2 attractor. Besides the second antisymmetric H4 and V4 modes (first and second POMs), the first symmetric (H1) and antisymmetric (H2) out-of-plane modes are also recognizable as those which could well (linearly) decompose the third and fourth POMs. Further, POMs show the involvement of third out-of-plane symmetric (H3) and first in-plane antisymmetric (V2) modes, too.

Table 2 summarizes dimensionality informations characterizing the motion classes recognized in the quasiperiodic scenario to chaos under out-of-phase support motion at 1/2-subharmonic resonance.

It is worth noticing that the first Hopf bifurcation relevant to the torus-breakdown scenario – i.e., the one bringing the periodic solution (P1-M2) to a (2T-QP1-M3) quasiperiodic motion – is associated with nearness of the excitation frequency to the 1/4-subharmonic resonance condition of the first torsion-symmetric mode $H1^T$. This resonance condition is rather sensitive to variations of the cable mechanical parameters: this is likely to be the reason why such scenario does not appear in the crossover cable.

3. Homoclinic bifurcation scenario

A scenario involving the global bifurcation of an *homoclinic* invariant set of a symmetric flow is responsible for transition to chaos with out-of-phase cable support motion (primary and 1/2-subharmonic resonance, in the latter case competing with the torus breakdown scenario described in Section 2.2), as well as with in-phase support motion (1/2-subharmonic resonance).

Homoclinic and heteroclinic orbits play an important role in dynamical systems behavior, and a theoretical framework (Glendinning and Sparrow, 1984; Shilnikov et al. 1998) can furnish an interpretative support to the experimental investigation.

Flows exhibiting homoclinic invariant sets exist at the upper bounds of stability regions of two-component periodic ballooning solutions VnHn with increasing frequency. This occurs with both antisymmetric ($n = 2, 4$) or symmetric ($n = 3, 5$) motions – for out-of-phase or in-phase support motion, respectively – whenever further components are not involved in the response before the bounds are reached. These ballooning motion classes are excited in primary external resonance conditions, although the frequency ranges where they occur are nominally labeled as primary ($n = 2$) or 1/2-subharmonic ($n = 3$–5) resonance zones following (Benedettini and Rega, 1997), the overall classification being done with respect to the first antisymmetric in-plane mode V2.

This scenario is concerned with each frequency zone where the ballooning-type classes of motion are present, independent of the support motion phase, for the slacker as well as the crossover cable. It shows to be robust with respect to variations of cable/mass geometric–mechanical parameters and thus it is of

general interest in the dynamics of the experimental system. Moreover, the bifurcation path relevant to in-phase support motion case is further enriched by the presence of heteroclinic bifurcation phenomena.

3.1. Out-of-phase support motion, primary and 1/2-subharmonic resonances

The bifurcation paths under out-of-phase support motion, whether relevant to primary or 1/2-subharmonic resonance, can be illustrated together due to their simile. In each case, the homoclinic invariant set manifests itself at the upper edge of the stability zone of an antisymmetric ballooning periodic solution, labeled VnHn, $n = 2, 4$.

In each frequency range (see Figs. 4 and 5 in Benedettini and Rega, 1997), the bifurcation analysis has been performed by varying the frequency of the support motion and keeping its amplitude as constant. The overall bifurcation path, schematically represented in Fig. 7(b) for the 1/2-subharmonic case, can be summarized as follows: for growing frequency, the one-modal periodic solution (P1) involving the Vn mode loses stability bifurcating towards ballooning periodic solutions (P2-M2) involving the Hn mode, too. Actually, two VnHn solutions coexist differing only due to clockwise or anticlockwise rotation of the orbit in the configuration plane (connected with the Vn–Hn phase shift sign) (Rega et al., 1997). For even higher frequency, the ballooning solution loses stability and the system enters the zone of nonregular response involving the homoclinic invariant set. Finally, the upper bound of this nonregular zone borders on one-modal (Vn) periodic response (P1), again.

The noninteger correlation dimension evaluated for the nonregular attractor in this region ranges from a bit more than 2 to a bit more than 3, and a value of about 0.11 is obtained for the maximum Lyapunov exponent.

In Fig. 9, a projection (in-plane vertical displacement versus vertical velocity) of a Poincaré map obtained for an exemplifying case in 1/2-subharmonic region is represented together with the relevant power spectrum.

Due to the nature of the involved phenomenon, the experimental characterization was concerned not only with the attractor global properties (dimension or strangeness) but also with the structure of the flow: in particular, presence and features (dimension and stability) of associated invariant sets were investigated. In fact, the characterization of invariant sets exhibited by the Poincaré section (in $\Re^3$) of the attractor reconstructed in $\Re^4$ (the singular value decomposition of the flow showing that four dimensions are sufficient

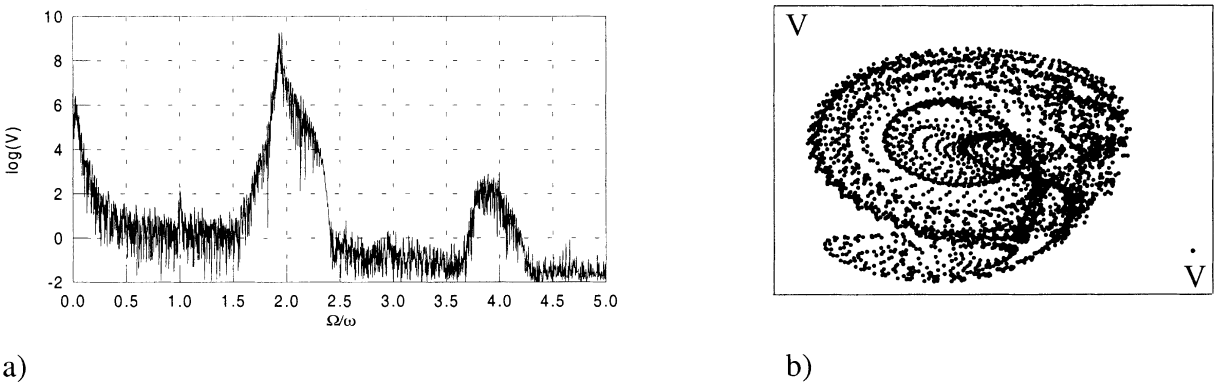

Fig. 9. (a) Power spectrum of horizontal component and (b) Poincaré map projection for a chaotic motion in the homoclinic scenario (out-of-phase support motion, 1/2-subharmonic resonance).

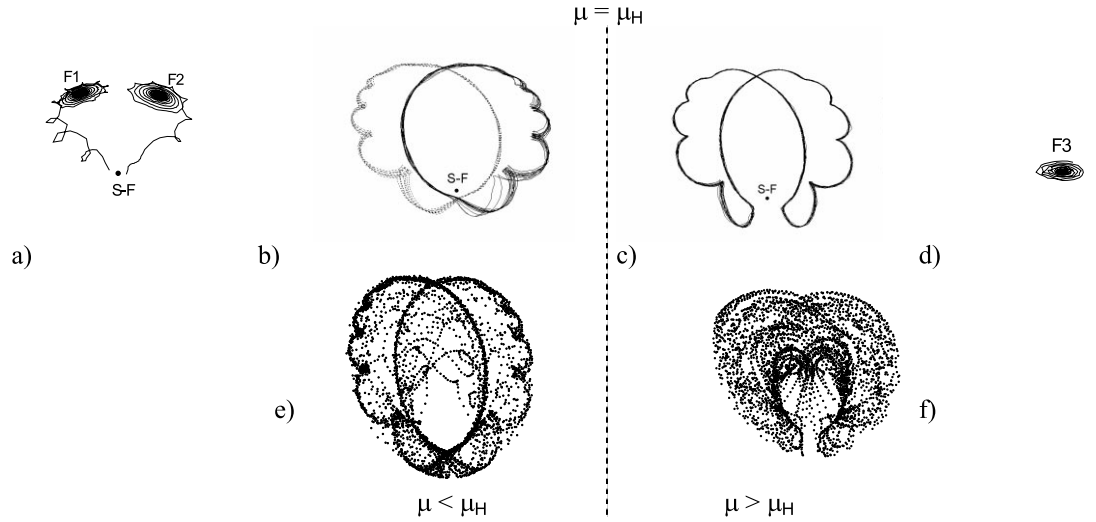

Fig. 10. Poincaré sections of the configuration space in the neighborhood of the homoclinic bifurcation. For control parameter values lower than the critical value μ_H: (a) two sets of dimension 0 symmetrically arranged, (b) two sets of dimension 1 asymmetric but symmetrically arranged. For control parameter values higher than the critical value μ_H: (c) one symmetric set of dimension 1, (d) one set of dimension 0. Close to the critical value: (e, f) non integer dimension, i.e. chaotic dynamics.

to describe meaningful system dynamics) allows us to describe, in depth, the interesting phenomenon displayed (Alaggio and Rega, 2000b).

In the neighborhood of the global bifurcation resulting to chaos, the flow looks like being organized by the instability of a one-dimensional invariant set (a saddle-focus type fixed point on the three-dimensional Poincaré map) and by the presence of an invariant set of dimension 2 homoclinic to the above mentioned fixed point. The characterization of the flow structure – which is enriched by the presence of the symmetry $f(x_1,x_2,x_3,x_4) = f(-x_1,-x_2,x_3,x_4)$ – allows us to point out (see Fig. 10, relevant to $n = 4$ case) the presence on the Poincaré section of the following invariant sets: (i) Two sets of dimension 1 (globally stable, locally unstable) asymmetric but symmetrically arranged (b), organized by one saddle-focus type fixed point (S-F), for control parameter values slightly lower than the critical value (homoclinic tangency, $\mu = \mu_H$). (ii) Two sets of dimension 0, two focus type fixed points (F_1, F_2) symmetrically arranged (a), on the same parameter side but farther away from the critical value (relevant to the two coexisting versions of periodic antisymmetric ballooning that will bifurcate toward the invariant sets identified at point (i) with growing parameter. (iii) One symmetric set of dimension 1 (globally stable, locally unstable) (c), organized by S-F type fixed point, for parameter values slightly higher than the critical value. (iv) One set of dimension 0, a focus type fixed point (F_3) (d), on the same side but farther away from μ_H (relevant to a symmetric orbit of periodic in-plane antisymmetric motion Vn).

Close to the critical value on the two sides of the parameter range, the experimental system exhibits chaotic dynamics (Fig. 10(e) and (f)), whose higher dimension ($D_C > 3$), major robustness and wider range are obtained for $\mu > \mu_H$.

The bifurcation behavior of the model can be set in the paradigm of homoclinic bifurcations as extended to symmetric flows by Glendinning and Sparrow (1984).

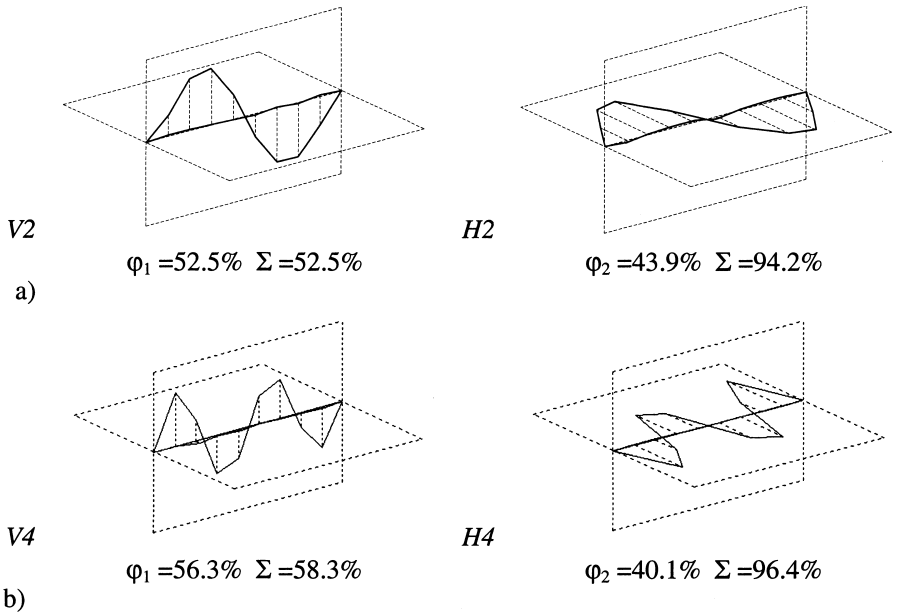

Fig. 11. First two POMs at (a) primary ($n = 2$) and (b) 1/2-subharmonic ($n = 4$) resonance, respectively.

Table 3
An overview of the motion class characterization[a]

Attractor	Dimension						Modes
	D_C	D_S	D_E	*D-T*	No. POMs	D_P	
Out-of-phase support motion – 1/2 subharmonic resonance homoclinic scenario							
P1-M2	1	2	$1 \div 3$	2^R	2	5	V4 H4
CH	$2.27 \rightarrow 3$	4	$3 \div 7$		2 (96.4%)	5	V4 H4
	$3 \leftarrow 3.11$	6	$4 \div 9$		2 (93.8%)	5	V4 H4
					3 (95.7%)	7	V4 H4 H2
Out-of-phase support motion – primary resonance homoclinic scenario							
P1-M2	1	2	$1 \div 3$	2^R	2	5	V2 H2
CH	2.39	4	$3 \div 7$		2 (94.2%)	5	V2 H2

[a] Refer footnote of Table 1.

When the cable model follows the aforementioned scenario, the chaotic attractors show the lowest observed dimensionality: indeed, the transition from regular to nonregular behavior happens without increasing the number of involved modes over the two (Vn, Hn) already present in the neighboring regular zones. The POD of two experimental series ($n = 2,\ 4$) corresponding to chaotic attractors gives the results shown in Fig. 11: more than 94% and 96% of the signal power that belongs to the two POMs (Vn and Hn), already responsible for the regular ballooning, respectively. Fully developed chaos for 1/2-subharmonic resonance condition ($n = 4,\ D_C = 3.11$) also shows a small contribution from first out-of-plane antisymmetric H2 mode.

Table 3 summarizes the informations characterizing the motion classes recognized in the homoclinic bifurcation scenario at 1/2-subharmonic and primary resonance.

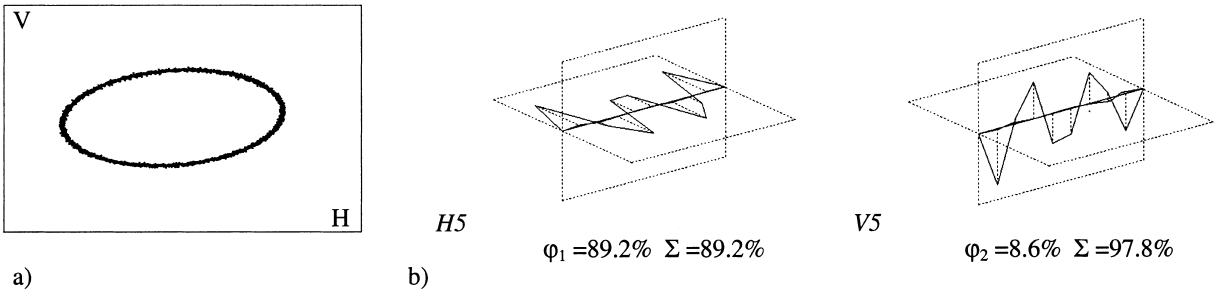

Fig. 12. (a) Symmetric ballooning V5H5 in the configuration plane and (b) first two POMs (in-phase support motion, 1/2-subharmonic resonance).

3.2. In-phase support motion, 1/2-subharmonic resonance

The bifurcation analysis has been performed by varying the frequency of support motion in the range 2.2–2.6 (see Fig. 1 in Benedettini and Rega, 1997). Also in the case of in-phase support motion, 1/2-subharmonic resonance, transition to chaos involves the global bifurcation of an homoclinic invariant set, but now the scenario is even more enriched by the presence of a further phenomenon of *heteroclinic* tangency.

The bifurcation path follows the main route already depicted in Section 3.1 starting from a one-modal response (Vn), bifurcating in a ballooning solution – one of two coexisting (clockwise and counter-clockwise) and symmetrically arranged ballooning solutions VnHn, $n = 5$ – and ending in a region of nonregular regime in the neighborhood of the global bifurcation.

In Fig. 12, the ballooning motion class is exemplified by means of a projection of its configuration plane and relevant POMs. The ensuing nonregular dynamics exhibit a class of attractors topologically similar to those corresponding to the $n = 2$ and $n = 4$ cases.

However, an interesting difference seems to occur with respect to the "pure" homoclinic bifurcation phenomenon of Section 3.1. A second class of nonregular attractors coexists in the overall scenario. Evolving in parameter space, the fixed points (stable foci), already representative of the two ballooning periodic solutions VnHn ($n = 5$), still exhibit the spiraling stable manifold, which adds to the unstable one in a narrow frequency range. The unstable manifold injects the flow onto the stable manifold of the coexisting S-F fixed point singled out in the homoclinic scenario (Fig. 10), which in turn reinjects it back onto the other S-F. This situation is represented in Fig. 13(a)–(c), where the Poincaré section of two coexisting asymmetric attractors (a, b) and of one symmetric attractor (c) are shown. It configures an heteroclinic tangency to be further investigated, and produces a second family of attractors again made up of symmetric and antisymmetric invariant sets following the framework of the main scenario in Section 3.1.

The power spectrum (Fig. 13(d)) holds trace of the time spent by the system in going away from S-F$_i$ ($i = 1, 2$) in the harmonics organized in a quasiperiodic-like structure having ratio near to 3. The signal power relevant to the first two POMs in chaotic regime (H5: $\varphi_1 = 89.2\%, \Sigma = 89.2\%$; V5: $\varphi_2 = 8.6\%, \Sigma = 97.8\%$) is substantially unaltered with respect to that in Fig. 12(b) (periodic regime) while Table 4 summarizes the usual informations relevant to the motion classes.

4. Summary and discussion

Mechanisms of bifurcation to nonregular motions of an experimental cable/mass system hanging at sinusoidally in-phase or out-of-phase in-plane moving supports have been investigated. The system exhibits a rich variety of 2T- and 3T-quasiperiodic responses, chaos ensuing from tori breakdown, phase locking

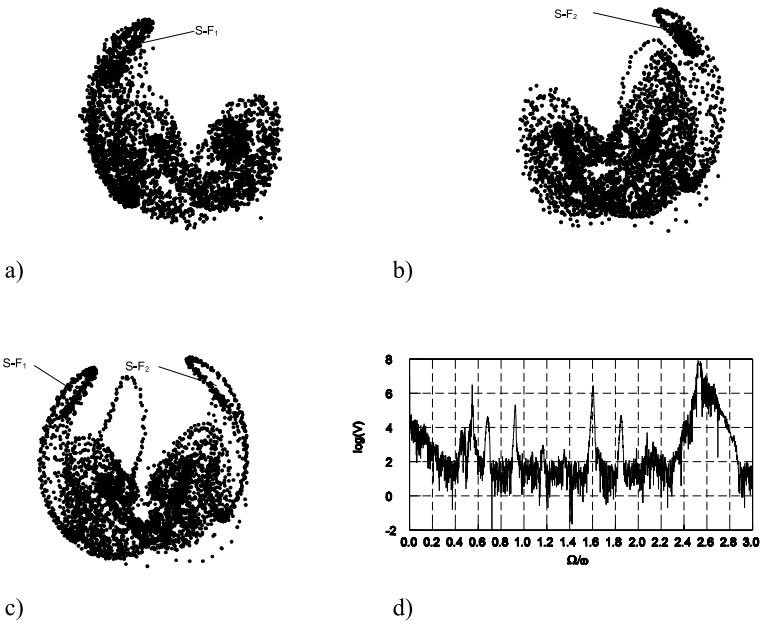

Fig. 13. Mixed heteroclinic–homoclinic bifurcation phenomenon: (a, b) Poincaré sections of two coexisting asymmetric attractors and (c) of one symmetric attractor. (d) Power spectrum.

Table 4
An overview of the motion class characterization[a]

Attractor	Dimension						Modes
	D_C	D_S	D_E	*D-T*	No. POMs	D_P	
In-phase support motion – 1/2-subharmonic resonance							
P1	1	2	$1 \div 3$	1	1 (96.2%)	3	V5
P2-M2	1	2	$1 \div 3$	2^R	2 (97.8%)	5	V5 H5
CH1	$2.30 \div 2.88$	4	$3 \div 7$		2 (96.8%)	5	V5 H5
					3 (98.1%)	7	V5 H5 H4
CH2	$3.04 \div 3.20$	6	$4 \div 9$		2 (91.1%)	5	V5 H5
					3 (98.2%)	7	V5 H5 H4

[a] Refer footnote of Table 1.

phenomena, homoclinic and heteroclinic bifurcations, depending on nearness to specific external/internal resonance conditions in the excitation parameter space.

Reconstructed attractors and underlying manifolds have been studied through a combined use of different techniques of experimental time series analysis, namely, delay embedding and POD techniques, focused at identifying mechanically meaningful classes of motion and actual associated mechanisms of transition to chaos. The embedding procedure allowed reliable estimates of the system dimensionality, with indications on the actual number of dof taking meaningful part in system's nonlinear dynamics. In turn, the POD procedure allowed us to characterize nonlinear responses not only in terms of the number of involved dof, but also with respect to their mechanical meaning. In particular, for each new dimension exhibited by the dynamics, a new experimental configuration variable has been identified as the one responsible for bifurcation and ensuing steady regime. This has been made in a number of meaningful transition regions from regular to nonregular responses.

Systematic comparison was carried out between the upper bound limit $(2[D_C]+1)$ for the embedding dimension given by the Mané theorem (Mané, 1981), and the phase space dimension (D_P) in R^N evaluated, using POD results, as two times the number of identified POMs plus 1 (the time). The results obtained show

(i) agreement between the two dimensionality measures ($D_P = 2[D_C]+1$) for regular motion on ergodic tori (Pm, nT-QPm),
(ii) interesting dimensional features ($D_P > 2[D_C]+1$), when the motion develops on a partially or totally resonant tori (Pm-Mk, nT-QPm-Mk),
(iii) agreement ($D_P = 2[D_C]+1$) for nonregular responses, provided a minimal number of POMs is included.

Though the system is potentially infinite-dimensional, its complex response was actually seen to be *low-dimensional* in most cases. Indeed, more than 90% of nonregular signal power is representable by using up to three or four POMs among those already responsible for the higher-dimensional coupled regular dynamics. In addition, an overall heuristic correspondence between the main POMs and the main linear *physical* modes of the system was highlighted.

These results are of notable interest to the aim of associating to each class of complex response of the system, a class of *reduced* (and minimal) theoretical models able to describe the complex dynamics of the experimental system. Within the framework of a reduction (discretization) procedure, these can specifically be built in each region of control parameter space either by using just the identified POMs, or getting hints from them by projecting infinite-dimensional dynamics on the known sub-optimal basis of corresponding linear modes.

A summary of results concerned with bifurcation to chaos scenarios and involved cable experimental modes is given in Table 5, making reference to features of support motion and external resonance condition, as well as to cable dynamic properties.

(a) *Quasiperiodic transition* to chaos via breakdown of regular dynamics on 3D-tori is robust for the slacker cable at primary resonance under in-phase support motion. This scenario looks rich and involved due to complicated interaction between internally resonant and nonresonant modes. Many classes of regular and nonregular response differing with respect to topological dimension, underlying manifold, and increasing number of configuration variables, have been highlighted. They involve well identified experimental eigenfunctions constituting the optimal basis for decomposing the spatio-temporal flow. Specifically, the first antisymmetric out-of-plane mode (H2) plays the decisive role as regards transition to chaos. This suggests a three-mode mathematical model including V1, H1 and H2 – like the one in (Benedettini

Table 5
Summary of nonregular regime zones, corresponding transition scenarios, and involved configuration variables – transition to nonregular dynamics

Cable	Support motion							
	In-phase external resonance condition				In opposition of phase external resonance condition			
	Primary		Subh. 1/2		Primary		Subh. 1/2	
	Scenario	Modes	Scenario	Modes	Scenario	Modes	Scenario	Modes
Slacker	QP	V1 H1 H2	HOM (HET)	V5 H5 V3 H3	HOM	V2 H2	HOM (QP)	V4 H4[a]
Crossover	No chaos		HOM	V5 H5 V3 H3	HOM	V2 H2	HOM	V4 H4

[a] V4 H4 H1^T H2.

et al., 1995), containing also a fourth mode, here unnecessary – could be sufficient to capture the important nonregular dynamics of the system in the considered frequency range.

It is worth noticing how, with the same excitation conditions, the quasiperiodic scenario to chaos does not occur for the crossover cable. Indeed, in this case, the existence of a nearly perfect 2:2:1:2 internal resonance involving all first four in-plane and out-of-plane, symmetric and antisymmetric, modes makes periodic coupled responses more robust, while preventing quasiperiodicity and chaos from occurrence.

For the slacker cable at 1/2-subharmonic resonance under out-of-phase motion, the quasiperiodic scenario competes with the homoclinic bifurcation scenario. Herein, the main role in transition to chaos is played by the first torsional symmetric out-of-plane mode ($H1^T$).

(b) The *homoclinic bifurcation* scenario to chaos is associated with passage from ballooning-type periodic motion to substantially unimodal motion. It is even more general in the dynamics of the experimental model. Indeed, it is definitely robust near primary resonances of 1:1 internally resonant VnHn-type couples of modes ($n = 2$–5; $n =$ odd, symmetric; $n =$ even, antisymmetric), for both the slacker and the crossover cable.

In particular, strong evidence is obtained about the importance of (i) first (second) in-plane and out-of-plane antisymmetric modes at regions of primary (1/2-subharmonic) nominal resonance of V1, when out-of-phase support motion is considered; (ii) higher-order in-plane and out-of-plane symmetric modes, when in-phase support motion at 1/2-subharmonic nominal resonance of V1 is considered. In all cases, hints are obtained about possible construction of 2-mode mathematical models accounting for V2, H2 (V4, H4) in the former case, and for V5, H5 or V3, H3 in the latter case. Of course, in defining such mathematical models, account should also be taken of the likely need to include the basic symmetric in-plane mode (V1), too: indeed, this cannot be omitted, e.g., in the case of antisymmetric models, since antisymmetric modes cannot actually be excited in even regularly coupled motion unless a cable dynamic tension mechanism be properly induced by any symmetric mode (Rega et al., 1997).

Finally, it is worth observing that the homoclinic bifurcation phenomenon is even further enriched by the presence of heteroclinic bifurcation for the slacker cable at 1/2-subharmonic resonance under in-phase motion.

References

Abarbanel, H.D.I., Brown, R., Sidorowich, J.J., Tsimring, L.S., 1993. The analysis of observed chaotic data in physical systems. Reviews of Modern Physics 65 (4), 1331–1392.

Alaggio, R., Rega, G., 2000a. Characterizing bifurcations and classes of motion in the transition to chaos through 3D-tori of a continuous experimental system in solid mechanics. Physica D, 137(1–2), 70–93.

Alaggio, R., Rega, G., 2000b, in prepararation.

Anishchenko, V.S., Safonova, M.A., Feudel, U., Kurths, J., 1994. Bifurcations and transition to chaos through three-dimensional tori. International Journal of Bifurcation and Chaos 4 (3), 595–607.

Baesens, C., Guckenheimer, J., Kim, S., MacKay, R.S., 1991. Three coupled oscillators: mode-locking, global bifurcation and toroidal chaos. Physica D 49 (3), 387–475.

Battelino, P.M., Grebogi, C., Ott, E., Yorke, J.A., 1989. Chaotic attractors on a 3-torus, and the torus break-up. Physica D 39 (2–3), 299–314.

Benedettini, F., Rega, G., 1997. Experimental investigation of the nonlinear response of a hanging cable. Part II: Global analysis. Nonlinear Dynamics 14 (2), 119–138.

Benedettini, F., Rega, G., Alaggio, R., 1995. Non-linear oscillations of a four-degree-of-freedom model of a suspended cable under multiple internal resonance conditions. Journal of Sound Vibration 182 (5), 775–798.

Broomhead, D.S., King, G.P., 1986. Extracting qualitative dynamics from experimental data. Physica D 20 (2–3), 217–236.

Cusumano, J.P., Sharkady, M.T., Kimble, B.W., 1994. Experimental measurements of dimensionality and spatial coherence in the dynamics of a flexible-beam impact oscillator. Philosophical Transactions of the Royal Society of London A 347, 421–434.

Eckmann, J.P., Ruelle, D., 1985. Ergodic theory of chaos and strange attractors. Reviews of Modern Physics 57 (3), 617–656.

Georgiou, I.T., Schwartz, I.B., 1999. Dynamics of large scale coupled structural/mechanical systems: a singular perturbation/proper orthogonal decomposition approach. SIAM Journal on Applied Mathematics 59 (4), 1178–1207.

Giberti, C., Zanassi, R., 1993. Behaviour of a three-torus in truncated Navier–Stokes equations. Physica D 65, 300–312.

Glendinning, P., Sparrow, C., 1984. Local and global behaviour near homoclinic orbits. Journal of Statistical Physics 35 (5–6), 645–696.

Grassberger, P., Procaccia, I., 1983. Characterization of strange attractors. Physics Review Letters 50 (5), 346–349.

Grebogi, C., Ott, E., Yorke, J., 1985. Attractors on an n-torus: quasiperiodicity versus chaos. Physica D 15 (3), 354–373.

Holmes, P., Lumley, J.L., Berkooz, G., 1996. Turbolence, Coherent Structures, Dynamical Systems and Symmetry. Cambridge Monographs on Mechanics. Cambridge University Press, Cambridge.

Holzfuss, J., Lauterborn, W., 1989. Lyapunov exponents from a time series of acoustic chaos. Physical Review A 39 (4), 2146–2152.

Irvine, H.M., Caughey, T.K., 1974. The linear theory of free vibrations of a suspended cable. Proceedings of the Royal Society of London A 341, 299–315.

Mané, R., 1981. On the dimension of the compact invariant sets of certain nonlinear maps. In: Dynamical Systems and Turbulence. Springer Lecture Notes in Mathematics, Springer, Berlin, pp. 230–242.

Newhouse, S., Ruelle, D., Takens, F., 1978. Occurrence of strange axiom-A attractors near quasiperiodic flows on T^m $m \geqslant 3$. Communications in Mathematical Physics 64 (1), 35–40.

Packard, N.H., Crutchfield, J.P., Farmer, J.D., Shaw, R.S., 1980. Geometry from a time series. Physics Review Letters 45, 712.

Rega, G., Alaggio, R., Benedettini, F., 1997. Experimental investigation of the nonlinear response of a hanging cable. Part I: Local analysis. Nonlinear Dynamics 14 (2), 89–117.

Ruelle, D., Takens, F., 1971. On the nature of turbulence. Communications in Mathematical Physics 20, 167–192.

Sauer, T., Yorke, J.A., Casdagli, M., 1991. Embedology. Journal of Statistical Physics 65 (3–4), 579–616.

Shilnikov, L., Shilnikov, A., Turaev, D., O Chua, L., 1998. Methods of Qualitative Theory in Nonlinear Dynamics. World Scientific Series on Nonlinear Science Series A (4). World Scientific, Singapore.

Steindl, A., Troger, H., Zemann, V., 1999. Improved Galerkin method in the dimension reduction of nonlinear dynamical systems. In: New Application of Nonlinear and Chaotic Dynamics in Mechanics. Kluwer Academic Publishers, London, pp. 71–80.

Takens, F., 1981. Detecting strange attractors in turbolence. In: Dynamical Systems and Turbulence. Springer Lecture Notes in Mathematics (898). Springler, Berlin, pp. 366–381.